Advances in Difference Equations
a SpringerOpen Journal

RESEARCH Open Access

Hybrid variational model based on alternating direction method for image restoration

Jianguang Zhu[1], Kai Li[1] and Binbin Hao[2*]

*Correspondence:
bbhao981@163.com
[2]College of Science, China University of Petroleum, Qingdao, P.R. China
Full list of author information is available at the end of the article

Abstract

The total variation model is widely used in image deblurring and denoising process with the features of protecting the image edge. However, this model usually causes some staircase effects. To overcome the shortcoming, combining the second-order total variation regularization and the total variation regularization, we propose a hybrid total variation model. The new improved model not only eliminates the staircase effect, but also well protects the edges of the image. The alternating direction method of multipliers (ADMM) is employed to solve the proposed model. Numerical results show that our proposed model can get more details and higher image visual quality than some current state-of-the-art methods.

Keywords: Total variation; Image restoration; Staircase effect; Alternating direction method of multipliers

1 Introduction

Image restoration mainly includes image deblurring and image denoising, which is one of the most fundamental problems in imaging science. It plays an important role in many mid-level and high-level image-processing areas such as medical imaging, remote sensing, machine identification, and astronomy [1–4]. The image restoration problem usually can be expressed in the following form:

$$g = Hf + \eta, \tag{1.1}$$

where $f \in R^{n^2}$ is the original $n \times n$ image, $H \in R^{n^2 \times n^2}$ is a blurring operator, $\eta \in R^{n^2}$ is the white Gaussian noise, and $g \in R^{n^2}$ is a degraded image.

It is well known that the image restoration problem is usually an ill-posed problem. An efficient method to overcome the ill-posed problems is to add some regularization terms to the objective functions, which is known as a regularization method. There are two famous regularization methods. One is the Tikhonov regularization [5], and the other is the total variation (TV) regularization [6]. The Tikhonov regularization method has a disadvantage, which tends to make images overly smooth and often fails to adequately preserve important image attributes such as sharp edges. The total variation regularization method has the ability to preserve edges well and remove noise at the same time, which was first

introduced by Rudin et al. [6] as follows:

$$\min_f \|Hf - g\|_2^2 + \alpha \|f\|_{\mathrm{TV}}, \tag{1.2}$$

where $\|\cdot\|_2$ denotes the Euclidean norm, $\|\cdot\|_{\mathrm{TV}}$ is the discrete total variation regularization term, and α is a positive regularization parameter that controls the tradeoff between these two terms. To define the discrete TV norm, we first introduce the discrete gradient ∇f:

$$(\nabla f)_{i,j} = \left((\nabla f)_{i,j}^x, (\nabla f)_{i,j}^y\right)$$

with

$$(\nabla f)_{i,j}^x = \begin{cases} f_{i+1,j} - f_{i,j} & \text{if } i < n, \\ f_{1,j} - f_{n,j} & \text{if } i = n, \end{cases} \qquad (\nabla f)_{i,j}^y = \begin{cases} f_{i,j+1} - f_{i,j} & \text{if } j < n, \\ f_{i,1} - f_{i,n} & \text{if } j = n, \end{cases}$$

for $i, j = 1, \ldots, n$. Here $\nabla : \Re^{n^2} \to \Re^{n^2}$ denotes the discrete gradient operator, $f_{i,j}$ refers to the $((j-1)n + i)$th entry of the vector f, which is the (i,j)th pixel location of the image; see [7]. Then the discrete TV of f is defined by

$$\|f\|_{\mathrm{TV}} = \sum_{1 \le i,j \le n} \sqrt{\left|(\nabla f)_{i,j}^x\right|^2 + \left|(\nabla f)_{i,j}^y\right|^2}.$$

Due to the nonlinearity and nondifferentiability of the total variation function, it is difficult to solve model (1.2). To solve this problem more effectively, many methods have been proposed for total-variation-based image restoration in recent years [6–27]. In these methods, Rudin et al. [6] raised a time marching scheme, and Vogel et al. [7] put forward a fixed point iteration method. The time marching scheme converges slowly, especially when the iterate point is close to the solution set. The fixed point iteration method is also very difficult to solve as the blurring kernel becomes larger. Based on the dual formulation, Chambolle [15] proposed a gradient algorithm for the total variation denoising problem. At present, based on variable separation and penalty techniques, Wang et al. [16] proposed the fast total variant deconvolution (FTVd) method. By introducing an auxiliary variable to replace the nondifferentiable part of model (1.2), the TV model (1.2) can be rewritten in the following minimization problem:

$$\min_{f,\omega} \|Hf - g\|_2^2 + \alpha \|\omega\|_2 + \frac{\beta}{2} \|\omega - \nabla f\|_2^2,$$

where β is a penalty parameter. Experimental results verify the effectiveness of the FTVd method. But in the calculation, the penalty parameter β needs to approach infinity, which creates numerical instability. To avoid the approach of penalty parameter to infinity, Chan et al. [28] proposed the alternating direction method of multipliers (ADMM) to solve model (1.2). By defining the augmented Lagrange function, the image restoration model (1.2) can be translated into the following form:

$$\min_{f,\omega} \|Hf - g\|_2^2 + \alpha \|\omega\|_2 + \langle \lambda, \omega - \nabla f \rangle + \frac{\beta}{2} \|\omega - \nabla f\|_2^2,$$

where λ is a Lagrange multiplier. The experimental results show that the ADMM method is robust and fast, and has a good restoration effect.

More recently, to overcome the shortcoming of the TV norm of f in model (1.2), Huang et al. [29] proposed a fast total variation minimization method for image restoration as follows:

$$\min_{f,u} \|Hf - g\|_2^2 + \alpha_1 \|f - u\|_2^2 + \alpha_2 \|u\|_{\mathrm{TV}}, \tag{1.3}$$

where α_1, α_2 are positive regularization parameters. Model (1.3) adds a term $\|f - u\|_2^2$, compared with model (1.2). The experimental results show that the modified TV minimization model can preserve edges very well in the image restoration processing. Based on model (1.3), Liu et al. [30] proposed the following minimization model:

$$\min_{f,u} \|Hf - g\|_2^2 + \alpha_1 \|f - u\|_2^2 + \alpha_2 \|f\|_{\mathrm{TV}} + \alpha_3 \|u\|_{\mathrm{TV}}, \tag{1.4}$$

where α_1, α_2, and α_3 are positive regularization parameters. Liu et al. [30] adopted the split Bregman method and Chambolle projection algorithm to solve the minimization model (1.4). Numerical results illustrated the effectiveness of their model.

Although the total variation regularization can preserve sharp edges very well, it also causes some staircase effects [31, 32]. To overcome this kind of staircase effect, some high-order total variational models [33–39] and fractional-order total variation models [40–44] are introduced. It has been proved that the high-order TV norm can remove the staircase effect and preserve the edges well in the process of image restoration.

To eliminate the staircase effect better and preserve edges very well in image processing, we combine the TV norm and second-order TV norm and introduce a new hybrid variational model as follows:

$$\min_{f,u} \|Hf - g\|_2^2 + \alpha_1 \|f - u\|_2^2 + \alpha_2 \left\|\nabla^2 f\right\|_2 + \alpha_3 \|\nabla u\|_2, \tag{1.5}$$

where α_1, α_2, and α_3 are positive regularization parameters, $\|\nabla u\|_2$ is the TV norm of u, and $\|\nabla^2 f\|_2$ is the second-order TV norm of f. The definition of the second-order TV norm is similar to that of the TV norm. The second-order TV norm is defined by

$$\begin{aligned}
&\left(\nabla^2 f\right)_{i,j} = \left((\nabla f)_{i,j}^{x,x}, (\nabla f)_{i,j}^{x,y}, (\nabla f)_{i,j}^{y,x}, (\nabla f)_{i,j}^{y,y}\right),\\
&\left\|\nabla^2 f\right\| = \sum_{1\le i,j\le n} \sqrt{\left|(\nabla f)_{i,j}^{x,x}\right|^2 + \left|(\nabla f)_{i,j}^{x,y}\right|^2 + \left|(\nabla f)_{i,j}^{y,x}\right|^2 + \left|(\nabla f)_{i,j}^{y,y}\right|^2},
\end{aligned}$$

where $(\nabla f)_{i,j}^{x,x}$, $(\nabla f)_{i,j}^{x,y}$, $(\nabla f)_{i,j}^{y,x}$, $(\nabla f)_{i,j}^{y,y}$ denote the second-order differences of the $((j-1)n+i)$th entry of the vector f. For more detail about the second-order differences, we refer to [45]. The second-order TV regularization and TV regularization are used; the edges in the restored image can be preserved quite well, and the staircase effect is reduced simultaneously.

The rest of this paper is organized as follows. In Sect. 2, we propose our alternating iterative algorithm to solve model (1.5). In Sect. 3, we give some numerical results to demonstrate the effectiveness of the proposed algorithm. Finally, concluding remarks are given in Sect. 4.

2 The alternating iterative algorithm

In this section, we use an alternating iterative algorithm to solve (1.5). Based on the variable separation technique [16], the minimization problem (1.5) can be divided into deblurring and denoising steps. The alternating iterative algorithm is based on decoupling of denoising and deblurring steps in the image restoration process. The deblurring step is defined as

$$\arg\min_{f} \|Hf - g\|_2^2 + \alpha_1 \|f - u\|_2^2 + \alpha_2 \left\| \nabla^2 f \right\|_2. \tag{2.1}$$

The denoising step is defined as

$$\arg\min_{u} \alpha_1 \|u - f\|_2^2 + \alpha_3 \|\nabla u\|_2. \tag{2.2}$$

We adopt the alternating direction multiplier method to solve these two subproblems.

2.1 The deblurring step

Because the ADMM method has the characteristics of notable stability and high rate of convergence, this method can avoid the approach of penalty parameter to infinity. We employ the alternating direction method of multipliers to solve the minimization problem (2.1). Because the objective function of (2.1) is nondifferentiable, by introducing an auxiliary variable ω, the unconstrained optimization problem (2.1) can be transformed into the following equivalent constraint optimization problem:

$$\arg\min_{f,\omega} \|Hf - g\|_2^2 + \alpha_1 \|f - u\|_2^2 + \alpha_2 \|\omega\|_2 \quad \text{s.t. } \omega = \nabla^2 f. \tag{2.3}$$

For the constrained optimization problem (2.3), its augmented Lagrange function is defined by

$$\begin{aligned} L_{\mathrm{A}}(f, \omega, \lambda_1) = {} & \|Hf - g\|_2^2 + \alpha_1 \|f - u\|_2^2 + \alpha_2 \|\omega\|_2 \\ & + \left\langle \lambda_1, \omega - \nabla^2 f \right\rangle + \frac{\beta_1}{2} \left\| \omega - \nabla^2 f \right\|_2^2, \end{aligned} \tag{2.4}$$

where λ_1 is a Lagrange multiplier, playing the role of avoiding the positive penalty parameters to go to infinity, and β_1 is a positive penalty parameter. Then, the alternating minimization method to minimize problem (2.4) can be expressed as follows:

$$\begin{cases} (f^{k+1}, \omega^{k+1}) = \arg\min_{f,\omega} L_A(f, \omega, \lambda_1^k), \\ \lambda_1^{k+1} = \lambda_1^k + \beta_1(\omega^{k+1} - \nabla^2 f^{k+1}). \end{cases} \tag{2.5}$$

Based on the classical ADMM, starting at $u = u^k$, $\omega = \omega^k$, $\lambda = \lambda^k$, the iterative scheme is implemented via the following subproblems:

$$f^{k+1} = \arg\min_f \{\|Hf - g\|_2^2 + \alpha_1 \|f - u^k\|_2^2 - \langle \lambda_1^k, \nabla^2 f \rangle + \frac{\beta_1}{2} \|\omega^k - \nabla^2 f\|_2^2\}, \tag{2.6}$$

$$\omega^{k+1} = \arg\min_\omega \{\alpha_2 \|\omega\|_2 + \langle \lambda^k, \omega \rangle + \frac{\beta_1}{2} \|\omega - \nabla^2 f^{k+1}\|_2^2\}, \tag{2.7}$$

$$\lambda_1^{k+1} = \lambda_1^k + \beta_1(\omega^{k+1} - \nabla^2 f^{k+1}). \tag{2.8}$$

Based on the optimal conditions, the solution of (2.6) is given by the equation

$$\left(2H^TH + \beta_1\nabla^{2^T}\nabla^2 + 2\alpha_1 I\right)f = 2H^Tg + 2\alpha_1 u^k + \beta_1\nabla^{2^T}\left(\omega^k + \frac{\lambda_1^k}{\beta_1}\right), \tag{2.9}$$

where ∇^{2^T} is the conjugate operator of ∇^2. Under the periodic boundary condition, H^TH and $\nabla^{2^T}\nabla^2$ are block circulant matrices [46, 47], so H^TH and $\nabla^{2^T}\nabla^2$ can be diagonalized by the Fourier transform. The Fourier transform of f is denoted by $\mathcal{F}(f)$, and $\mathcal{F}^{-1}(f)$ is the inverse Fourier transform of f. By using the Fourier transform the solution of f can be given as follows:

$$f^{k+1} = \mathcal{F}^{-1}(\gamma),$$

where

$$\gamma = \frac{\mathcal{F}(2H^Tg + 2\alpha_1 u^k + \beta_1\nabla^{2^T}(\omega^k + \frac{\lambda_1^k}{\beta_1}))}{\mathcal{F}(2\alpha_1 I + \beta_1\nabla^{2^T}\nabla^2 + 2H^TH)}.$$

The subproblem for ω can be written as

$$\omega^{k+1} = \arg\min_{\omega}\left\{\alpha_2\|\omega\|_2 + \frac{\beta_1}{2}\left\|\omega - \left(\nabla^2 f^{k+1} - \frac{\lambda_1^k}{\beta_1}\right)\right\|_2^2\right\},$$

and the solution can be explicitly obtained using the following two-dimensional shrinkage operator [16, 48]:

$$\omega^{k+1} = \max\left\{\left\|\nabla^2 f^{k+1} - \frac{\lambda_1^k}{\beta_1}\right\|_2 - \frac{\alpha_2}{\beta_1}, 0\right\}\frac{\nabla^2 f^{k+1} - \frac{\lambda_1^k}{\beta_1}}{\|\nabla^2 f^{k+1} - \frac{\lambda_1^k}{\beta_1}\|_2}, \tag{2.10}$$

where we follow the convention that $0 \cdot (0/0) = 0$.

Finally, we update λ_1 by

$$\lambda_1^{k+1} = \lambda_1^k + \eta\beta_1\left(\omega^{k+1} - \nabla^2 f^{k+1}\right), \tag{2.11}$$

where η is a relaxation parameter, and $\eta \in (0, (\sqrt{5}+1)/2)$.

The algorithm of the deblurring step is summarized in Algorithm 1.

2.2 The denoising step

Subproblem (2.2) is a classical TV regularization process for image denoising, which can be solved by the Chambolle projection algorithm. However, it is well known that the Chambolle projection algorithm has large amount of calculations in the process of experiment and causes numerical instability. To overcome the disadvantage of numerical instability and large amount of calculations of the Chambolle projection algorithm, in this paper, we adopt the alternating direction multiplier method to solve subproblem (2.2).

The solution process of subproblem (2.2) is the same as that of subproblem (2.1). First, introducing an auxiliary variable v, problem (2.2) can be transformed into the following

Algorithm 1 Alternating direction minimization method for solving subproblem (2.1)

1. Input: $g, K, \alpha_1 > 0, \alpha_2 > 0, \beta_1 > 0$
2. Initialization: $f^0 = g$, $\omega^0 = \nabla^2 f^0$
3. **While** "not converged", **Do**
4. Compute f^{k+1} from
   $f^{k+1} = \mathcal{F}^{-1}(\gamma)$.
5. Compute ω^{k+1} via
   $$\omega^{k+1} = \max\{\|\nabla^2 f^{k+1} - \tfrac{\lambda_1^k}{\beta_1}\|_2 - \tfrac{\alpha_2}{\beta_1}, 0\} \frac{\nabla^2 f^{k+1} - \frac{\lambda_1^k}{\beta_1}}{\|\nabla^2 f^{k+1} - \frac{\lambda_1^k}{\beta_1}\|_2}.$$
6. Update λ^{k+1} from
   $\lambda_1^{k+1} = \lambda_1^k + \eta\beta_1(\omega^{k+1} - \nabla^2 f^{k+1})$.
7. **End Do**
8. Output f^{k+1}

constraint minimization problem:

$$\min_{u,v} \alpha_1 \left\| u - f^{k+1} \right\|_2^2 + \alpha_3 \|v\|_2 \quad \text{s.t. } v = \nabla u. \tag{2.12}$$

Second, to use the alternating direction multiplier method to solve model (2.12), we define its augmented Lagrangian function

$$L_A(u, v, \lambda_2) = \alpha_1 \left\| u - f^{k+1} \right\|_2^2 + \alpha_3 \|v\|_2 + \langle \lambda_2, v - \nabla u \rangle + \frac{\beta_2}{2} \|v - \nabla u\|_2^2, \tag{2.13}$$

where β_2 is a positive penalty parameters, and λ_2 is a Lagrange multiplier.

The variables u, f, v are coupled together, so we separate this problem into two subproblems and adopt the alternating iteration minimization method. The two subproblems are given as follows.

The "u-subproblem" for v fixed:

$$\min_u \alpha_1 \left\| u - f^{k+1} \right\|_2^2 + \frac{\beta_2}{2} \left\| v^k - \nabla u \right\|_2^2 - \left\langle \lambda_2^k, \nabla u \right\rangle. \tag{2.14}$$

The "v-subproblem" for u fixed:

$$\min_v \frac{\beta_2}{2} \left\| v - \nabla u^k \right\|_2^2 + \left\langle \lambda_2^k, v \right\rangle + \alpha_3 \|v\|_2. \tag{2.15}$$

The minimizer of subproblem (2.14) can be simplified as

$$\min_u \alpha_1 \left\| u - f^{k+1} \right\|_2^2 + \frac{\beta_2}{2} \left\| v^k - \left(\nabla u + \frac{\lambda_2^k}{\beta_2} \right) \right\|_2^2, \tag{2.16}$$

and the minimization problem (2.16) can be solved by the following equation:

$$\left(2\alpha_1 I + \beta_2 \nabla^T \nabla\right) u = 2\alpha_1 f^{k+1} + \beta_2 \nabla^T v^k + \nabla^T \lambda_2^k. \tag{2.17}$$

Under the periodic boundary conditions, $\nabla^T \nabla$ is a block circulant matrix, So $\nabla^T \nabla$ is diagonalizable by the two-dimensional discrete Fourier transform.

Algorithm 2 Alternating direction minimization method for solving the subproblem (2.2)

1. Input: g, K, $\alpha_1 > 0$, $\alpha_3 > 0$, $\beta_2 > 0$
2. Initialization: $u^0 = g$, $v^0 = \nabla u^0$
3. **While** "not converged", **Do**
4. Compute u^{k+1} from (2.17)
5. Compute v^{k+1} via (2.19)
6. Update λ_2^{k+1} from (2.20)
7. **End Do**
8. Output u^{k+1}

Next, the minimization of (2.15) with respect to v is equivalent to the minimization problem

$$\min_v \frac{\beta_2}{2}\left\|v - \left(\nabla u^{k+1} - \frac{\lambda_2^k}{\beta_2}\right)\right\|_2^2 + \alpha_3\|v\|_2, \tag{2.18}$$

and the solution of (2.18) can be explicitly obtained by the two-dimensional shrinkage:

$$v^{k+1} = \max\left\{\left\|\nabla u^{k+1} - \frac{\lambda_2^k}{\beta_2}\right\|_2 - \frac{\alpha_3}{\beta_2}, 0\right\}\frac{\nabla u^{k+1} - \frac{\lambda_2^k}{\beta_2}}{\|\nabla u^{k+1} - \frac{\lambda_2^k}{\beta_2}\|_2}. \tag{2.19}$$

The Lagrange multiplier λ_2 is updated as follows:

$$\lambda_2^{k+1} = \lambda_2^k + \eta\beta_2\left(v^{k+1} - \nabla u^{k+1}\right), \tag{2.20}$$

where η is a relaxation parameter.

The algorithm of the denoising step is written in Algorithm 2.

3 Numerical experiments

This section presents some numerical examples, which show that the performance of our proposed algorithm to solve image restoration problems. In the following experiments, we compare our proposed method (HTV) with Fast-TV [29] and FNDTV methods [30]. All experiments are performed under Windows 7 and MATLAB 2012a running on a desktop with an core i5 Duo central processing unit at 2.50 GHz and 4 GB memory. The quality of the restoration results by different methods is compared quantitatively by using the peak-signal-to-noise ratio (PSNR) and structural similarity index metric (SSIM). Suppose g, f^0, and u are the observed image, the ideal image, and the restored image, respectively. Then, the BSNR, MSE, PSNR, and SSIM are defined as follows:

$$\mathrm{BSNR} = 20\log_{10}\frac{\|g\|_2}{\|\eta\|_2},$$

$$\mathrm{MSE} = \frac{1}{n^2}\sum_{i=0}^{n^2-1}\left(f^0(i) - u(i)\right)^2,$$

$$\mathrm{PSNR} = 20\log_{10}\frac{\mathrm{MAX}_{f^0}}{\sqrt{\mathrm{MSE}}},$$

$$\mathrm{SSIM} = \frac{(2\mu_{f^0}\mu_u + c_1)(2\sigma_{f^0u} + c_2)}{(\mu_{f^0}^2 + \mu_u^2 + c_1)(\sigma_{f^0}^2 + \sigma_u^2 + c_2)},$$

where η is the additive noise vector, n^2 is the number of pixels of image, MAX_{f^0} is the maximum possible pixel value of the f^0, $\bar{f}$ is the mean intensity value of f^0, μ_{f^0} is the mean value of the f^0, μ_u is the mean value of u, $\sigma_{f^0}^2$ and σ_u^2 are the variances of f^0 and u, respectively, and σ_{f^0u} is the covariance of f^0 and u, and c_1 and c_2 are stabilizing constants for near-zero denominator values. We will also use the SSIM index map to reveals areas of high/low similarity between two images; the whiter the SSIM index map, the closer the two images. Further details on SSIM can be founded in the pioneer work [49].

Four test images, "Cameraman", "Lena", "Baboon", and "Man", which are commonly used in the literature, are shown in Fig. 1. We test three kinds of blur, that is, Gaussian blur, average blur, and motion blur. These different blurring kernels can be builded by the function "fspecial" in the Matlab. The additive noise is a Gaussian noise in all experiments. In all tests, we add the Gaussian white noise of different BSNR to the blurred images. In our experiments, the stopping criterion is that the relative difference between the successive iteration of the restored image should satisfy the inequality

$$\frac{\|f^{k+1} - f^k\|_2}{\|f^k\|_2} \leq 1 \times 10^{-4},$$

where f^k is the computed image at the kth iteration of the tested method. In the following experiments, for our proposed method, we fixed the parameter $\alpha_2 = 1.3e{-}2$ for all experiments, $\alpha_1 = 1e{-}4$ (for Gaussian blur and average blur), $3e{-}4$ (for motion blur), $\alpha_3 = 1e{-}4$ (for Gaussian blur and average blur), $2e{-}4$ (for motion blur). For the parameters of FastTV and FNDTV, we refer to [29, 30]. The parameters for every compared method are selected from many experiments until we obtain the best PSNR values.

Figure 2 shows the experiment for Gaussian blur. We select the "Cameraman" image (256×256) as the test image, which is shown in Figure 1(a). The "Cameraman" image degraded by Gaussian blur with blur nucleus $9 * 9$ and a noise with BSNR = 35 is shown in Fig. 2(a). The recovered images by FastTV, FNDTV, and our method are shown in Fig. 2(b)–(d). To demonstrate the effectiveness of our method more intuitively, we enlarge some part of the three restored images, and the results of enlarged parts are shown in Fig. 2(e)–(h). We also show the SSIM index maps of the restored images recovered by

(a) Cameraman (b) Lenna (c) Baboon (d) Man

Figure 1 Test images

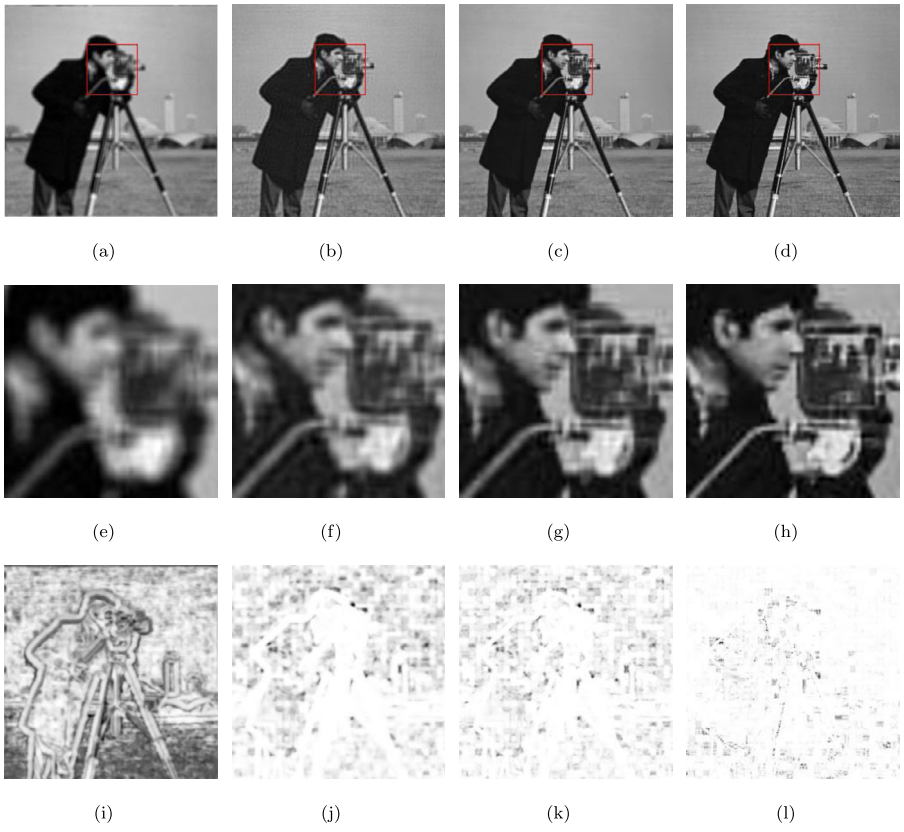

Figure 2 Results of different methods when restoring blurred and noisy image "Cameraman" degraded by Gaussian blur with Gaussian blur nucleus $9 * 9$ and a noise with $\mathrm{BSNR} = 35$: (**a**) blurred and noisy image; (**b**) restored image by FastTV; (**c**) restored image by FNDTV; (**d**) restored image by our method; (**e**) zoomed part of (**a**); (**f**) zoomed part of (**b**); (**g**) zoomed part of (**c**); (**h**) zoomed part of (**d**); (**i**) SSIM index map of the corrupted image; (**j**) SSIM index map of the recovered image by FastTV; (**k**) SSIM index map of the recovered image by FNDTV; (**l**) SSIM index map of the recovered image by our method

the three methods in Fig. 2(i)–(l). The SSIM map of the restored image by the proposed method is slightly whiter than the SSIM map by FastTV and FNDTV. The values of PSNR and SSIM by these methods are shown in Table 1. We see that both PSNR and SSIM values of the restored image by our proposed method are higher than FastTV and FNDTV. We also plot the changing curve of SSIM versus iterations with three different methods in Fig. 3. It is not difficult to see that our method can achieve a high SSIM over the other two methods with a few iterations. In addition, for the restoration effect of other images, we depict them by PSNRs and SSIMs; see Table 1. It is easy to detect that both of PSNR and SSIM of the restored image by our method are higher than others obtained by FastTV and FNDTV.

Figure 4 shows the experiment about the "Lenna" image with size 256×256 degraded by the average blur with length 9 and a noise with BSNR = 35. The degraded "Lenna" image is shown Fig. 4(a). The recovered images by FastTV, FNDTV, and our method are shown in Fig. 4(b)–(d). More precisely, Fig. 4(e)–(h) displays the same regions of special interest, which are zoomed in for comparing the performance of the three methods. It is not difficult to observe that the proposed method can alleviate the staircase phenomenon better. In addition, the SSIM map of the restored images recovered by the three meth-

Table 1 Experimental results for different images and different blur kernels, BSNR = 35

Image	Blur kernels	Fast-TV [26]		FNDTV [27]		Our	
		PSNR	SSIM	PSNR	SSIM	PSNR	SSIM
Cameraman	Gaussian(5, 5)	27.0656	0.4399	27.2341	0.4417	**27.8678**	**0.4562**
	Gaussian(7, 7)	26.1232	0.3992	26.8021	0.4155	**27.0689**	**0.4383**
	Gaussian(9, 9)	24.9719	0.3807	25.6502	0.4024	**26.4150**	**0.4057**
Couple	Gaussian(5, 5)	31.3219	0.7337	31.6776	0.7595	**32.8470**	**0.7889**
	Gaussian(7, 7)	29.9460	0.6767	30.7103	0.6989	**31.3003**	**0.7321**
	Gaussian(9, 9)	29.2731	0.6694	29.8778	0.6739	**30.6027**	**0.6963**
Lenna	average(7)	31.3460	0.6673	31.8335	0.6916	**32.6287**	**0.7256**
	average(9)	30.5242	0.6415	31.0531	0.6541	**31.6273**	**0.6737**
	average(11)	29.5574	0.6134	30.4395	0.6376	**30.9392**	**0.6481**
Goldhill	average(7)	28.3139	0.6077	29.2712	0.6188	**30.0464**	**0.6330**
	average(9)	28.1314	0.5816	28.3268	0.5990	**28.5740**	**0.6023**
	average(11)	26.8336	0.5244	27.4211	0.5576	**27.8857**	**0.5744**
Man	motion(20, 20)	29.8667	0.6258	30.1235	0.6622	**30.8716**	**0.6864**
	motion(10, 100)	30.5363	0.6839	31.2202	0.7130	**32.5163**	**0.7314**
Baboon	motion(20, 20)	27.4672	0.7968	27.8722	0.8334	**28.5560**	**0.8508**
	motion(10, 100)	28.8783	0.8213	28.9383	0.8621	**29.3343**	**0.8778**

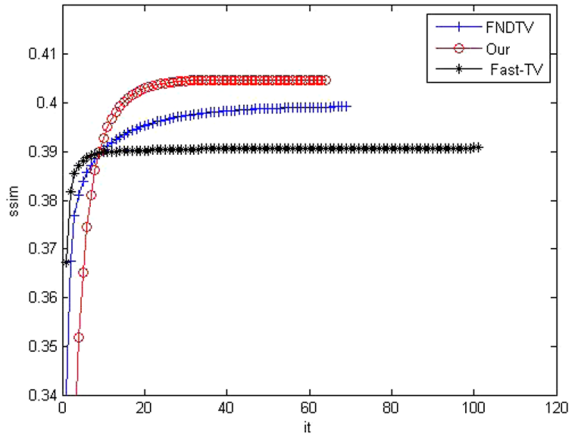

Figure 3 Changes of SSIM value versus iteration number for the three methods about Gaussian blur

ods is shown in Fig. 4(i)–(l). It is easy to see that the SSIM map obtained by the proposed method is slightly whiter than the maps by the other two methods. In Fig. 5, we plot the changes of SSIM value versus iteration number for the three methods. It can also be found from the relationship between SSIM values and iteration numbers that our method requires fewer iterations and the values are superior to the other two methods. These experiments demonstrate the outstanding performance of our proposed method to overcome the blocky images while preserving edge details. We also report the PSNR and SSIM values by these methods in Table 1. The PSNR and SSIM values of the restored image by our proposed method are higher than those of FastTV and FNDTV.

The experiments about the motion blur are shown in Figs. 6 and 8. On the motion blur, we do two groups of experiments for different thetas. one group of experiment is added serious degree of blur that is shown in Fig. 8, the other group of experiment is added slight degree of blur that is shown in Fig. 6. The recovered images by the three methods are shown in Figs. 6 and 8(b)–(d), and the enlarged parts are shown in Figs. 6 and 8(e)–

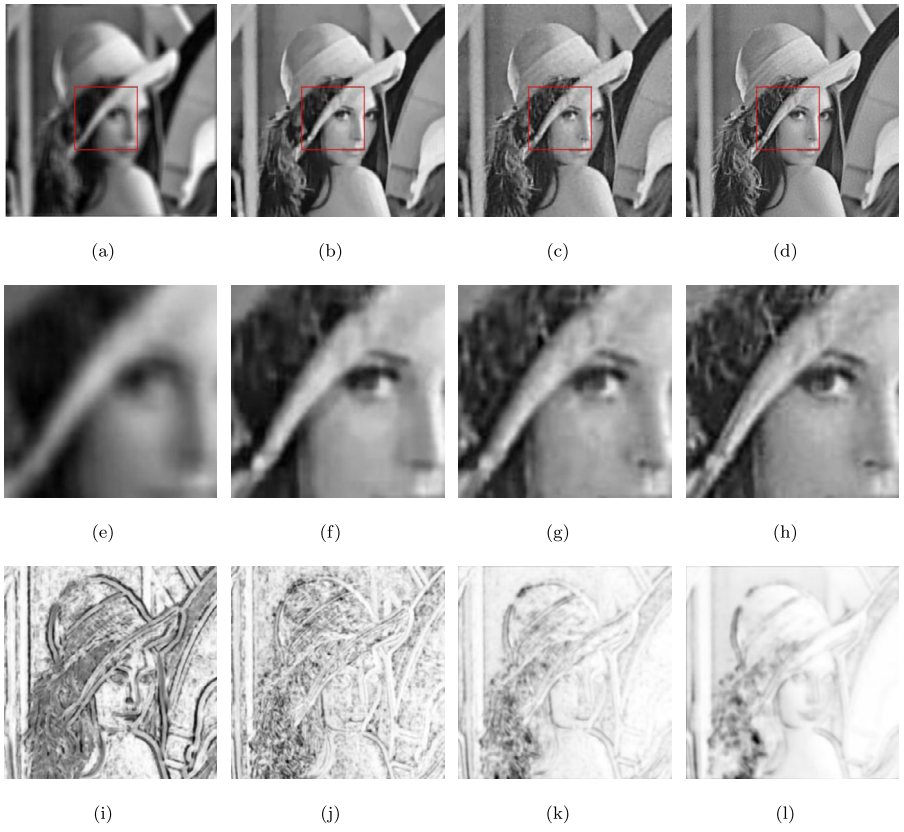

Figure 4 Results of different methods when restoring blurred and noisy image "Lenna" degraded by average blur with length 9 and a noise with $\mathrm{BSNR} = 35$: (**a**) blurred and noisy image; (**b**) restored image by Fast-TV; (**c**) restored image by FNDTV; (**d**) restored image by our method; (**e**) zoomed part of (**a**); (**f**) zoomed part of (**b**); (**g**) zoomed part of (**c**); (**h**) zoomed part of (**d**); (**i**) SSIM index map of the corrupted image; (**j**) SSIM index map of the recovered image by FastTV; (**k**) SSIM index map of the recovered image by FNDTV; (**l**) SSIM index map of the recovered image by our method

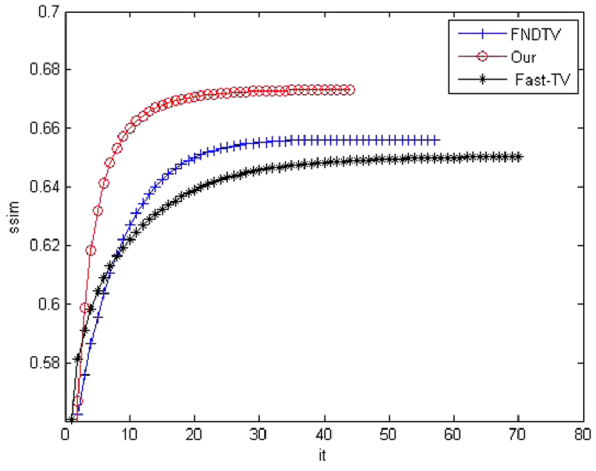

Figure 5 Changes of SSIM value versus iteration number for the three methods about average blur

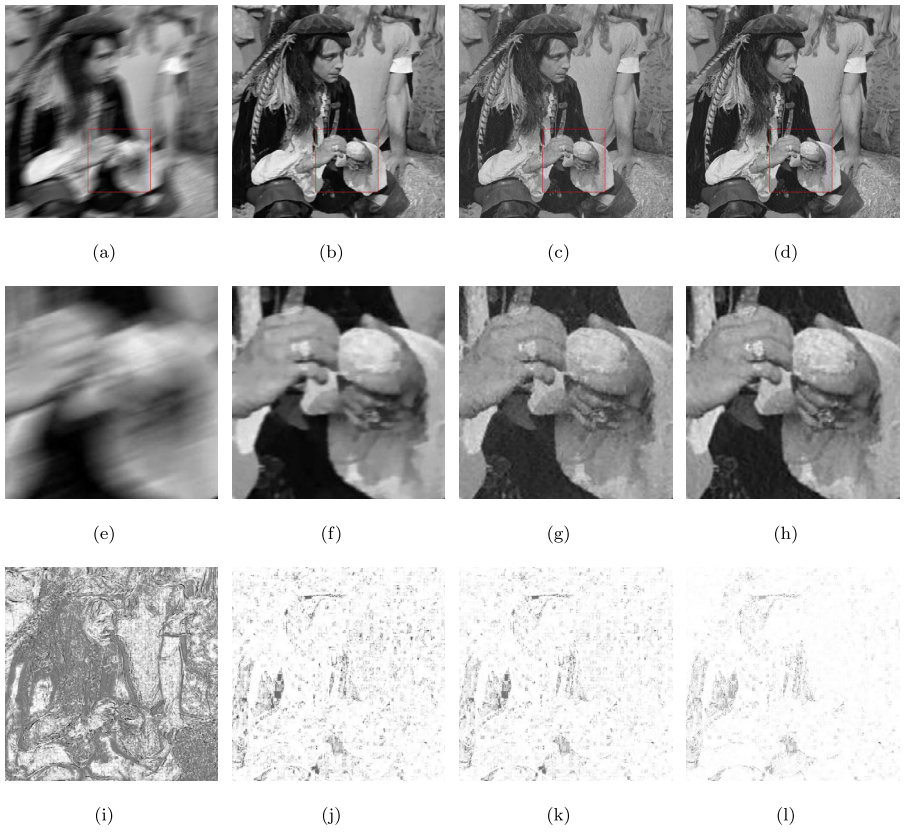

Figure 6 Results of different methods when restoring blurred and noisy image "Man" degraded by motion blur with **len** = 20 and **theta** = 20 and a noise with BSNR = 35: (**a**) blurred and noisy image; (**b**) restored image by Fast-TV; (**c**) restored image by FNDTV; (**d**) restored image by our method; (**e**) zoomed part of (**a**); (**f**) zoomed part of (**b**); (**g**) zoomed part of (**c**); (**h**) zoomed part of (**d**); (**i**) SSIM index map of the corrupted image; (**j**) SSIM index map of the recovered image by FastTV; (**k**) SSIM index map of the recovered image by FNDTV; (**l**) SSIM index map of the recovered image by our method

(h). We also show the SSIM index maps of the restored images recovered by the three methods in Figs. 6 and 8(j)–(l). It is easy to see that the SSIM map of the restored image by the proposed method is slightly whiter than the SSIM map by FastTV and FNDTV. In Figs. 7 and 9, we plot the changes of SSIMs with iteration number for FastTV method, FNDTV method, and our method. From Figs. 7 and 9, we can see that our method can get higher image visual quality and more details than Fast-TV method and FNDTV method. The values of PSNR and SSIM are listed in Tables 1 and 2. We see that both the PSNR and SSIM values of the restored image by the proposed method are much better than those provided by FastTV and FNDTV.

The numerical results of three different methods in terms of PSNR and SSIM are shown in the following tables. From Tables 1 and 2 it is not difficult to see that the PSNR and SSIM of the restored image by our proposed method are higher than those obtained by FastTV and FNDTV.

4 Conclusion

In this paper, we propose a hybrid total variation model. In addition, we employ the alternating direction method of multipliers to solve it. Experimental results demonstrate that

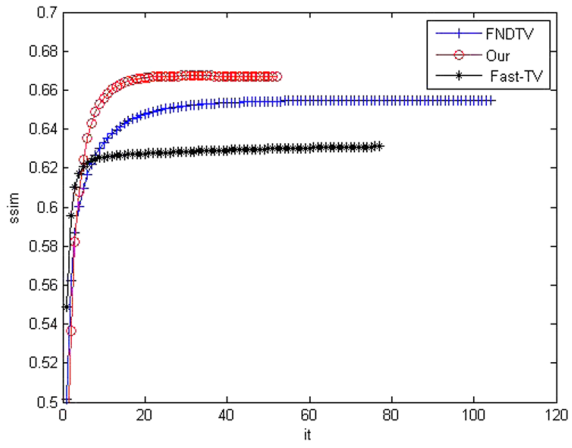

Figure 7 Changes of SSIM value versus iteration number for the three methods about motion blur with $\mathbf{theta} = 20$

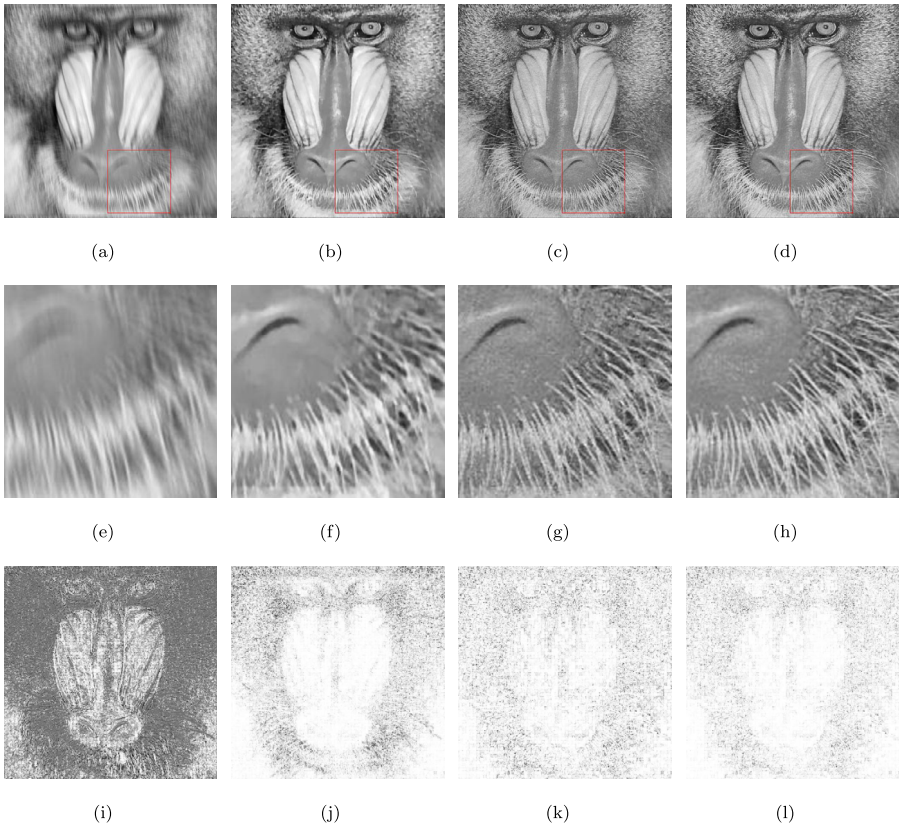

Figure 8 Results of different methods when restoring blurred and noisy image "Baboon" degraded by motion blur with $\mathbf{len} = 10$ and $\mathbf{theta} = 100$ and a noise with $\mathbf{BSNR} = 35$: (**a**) blurred and noisy image; (**b**) restored image by FastTV; (**c**) restored image by FNDTV; (**d**) restored image by our method; (**e**) zoomed part of (**a**); (**f**) zoomed part of (**b**); (**g**) zoomed part of (**c**); (**h**) zoomed part of (**d**); (**i**) SSIM index map of the corrupted image; (**j**) SSIM index map of the recovered image by FastTV; (**k**) SSIM index map of the recovered image by FNDTV; (**l**) SSIM index map of the recovered image by our method

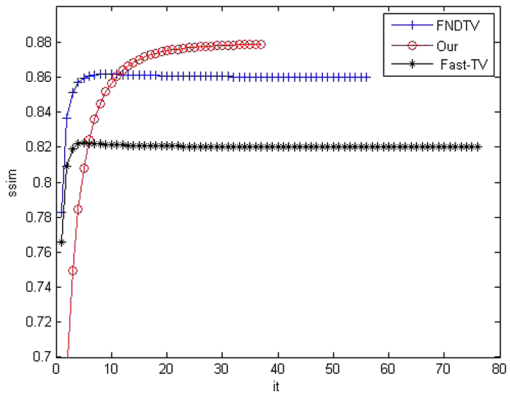

Figure 9 Changes of SSIM value versus iteration number for the three methods about motion blur with theta = 100

Table 2 Experimental results for different images and different blur kernels, BSNR = 40

Image	Blur kernels	Fast-TV [26]		FNDTV [27]		Proposed	
		PSNR	SSIM	PSNR	SSIM	PSNR	SSIM
cameraman	Gaussian(5, 5)	28.6897	0.4841	29.2310	0.5061	**29.6541**	**0.5208**
	Gaussian(7, 7)	27.4559	0.4427	27.0594	0.4369	**27.6590**	**0.4568**
	Gaussian(9, 9)	25.6219	0.4068	26.2835	0.4128	**27.3563**	**0.4435**
couple	Gaussian(5, 5)	32.0301	0.7718	32.8019	0.7942	**33.5144**	**0.8202**
	Gaussian(7, 7)	31.4577	0.7401	32.0764	0.7610	**32.6735**	**0.7797**
	Gaussian(9, 9)	30.1657	0.6786	30.9071	0.7011	**31.5687**	**0.7426**
lenna	average(7)	32.0735	0.7049	32.5344	0.7279	**33.3416**	**0.7526**
	average(9)	31.0432	0.6500	31.8694	0.6853	**32.7793**	**0.7312**
	average(11)	30.7127	0.6404	31.0552	0.6586	**31.3851**	**0.6724**
goldhill	average(7)	30.3156	0.6356	31.1560	0.6576	**32.0284**	**0.6920**
	average(9)	29.4280	0.6183	30.2251	0.6301	**31.4493**	**0.6656**
	average(11)	28.3722	0.6082	29.5978	0.6202	**30.6778**	**0.6464**
man	motion(20, 10)	30.7569	0.6720	31.3522	0.7031	**32.6930**	**0.7559**
	motion(11, 100)	31.6579	0.7234	32.1598	0.7398	**33.3935**	**0.8044**
baboon	motion(20, 10)	30.3003	0.8837	30.6833	0.8993	**31.5710**	**0.9128**
	motion(11, 100)	31.4377	0.9082	31.9844	0.9245	**32.5230**	**0.9323**

the proposed model can obtain better results than those restored by some existing restoration methods. It also shows that the new model can obtain a better visual resolution than the other two methods.

Acknowledgements
The authors would like to thank the referees for their valuable comments and suggestions.

Funding
This work was supported by National Key Research and Development Program of China (No. 2017YFC1405600), by the Training Program of the Major Research Plan of National Science Foundation of China (No. 91746104), by National Science Foundation of China (Nos. 61101208, 11326186), Qindao Postdoctoral Science Foudation (No. 2016114), Project of Shandong Province Higher Educational Science and Technology Program (No. J17KA166), Joint Innovative Center for Safe and Effective Mining Technology and Equipment of Coal Resources, Shandong Province of China and SDUST Research Fund (No. 2014TDJH102).

Competing interests
The authors declare that there is no conflict of interest regarding the publication of this paper.

Authors' contributions
All authors worked together to produce the results and read and approved the final manuscript.

Author details
[1]College of Mathematics and Systems Science, Shandong University of Science and Technology, Qingdao, P.R. China.
[2]College of Science, China University of Petroleum, Qingdao, P.R. China.

Publisher's Note

Received: 23 March 2018 Accepted: 2 December 2018 Published online: 28 January 2019

References

1. Hajime, T., Hayashi, T., Nishi, T.: Application of digital image analysis to pattern formation in polymer systems. J. Appl. Phys. **59**(11), 3627–3643 (1986)
2. Chen, M., Xia, D., Han, J., Liu, Z.: An analytical method for reducing metal artifacts in X-ray CT images. Math. Probl. Eng. **2019**, Article ID 2351878 (2019)
3. Chen, M., Li, G.: Forming mechanism and correction of CT image artifacts caused by the errors of three system parameters. J. Appl. Math. **2013**, Article ID 545147 (2013)
4. Chen, Y., Guo, Y., Wang, Y., et al.: Denoising of hyperspectral images using nonconvex low rank matrix approximation. IEEE Trans. Geosci. Remote Sens. **55**(9), 5366–5380 (2017)
5. Tikhonov, A.N., Arsenn, V.Y.: Solution of Ill-Posed Problem. Winston and Sons, Washington (1977)
6. Rudin, L.I., Osher, S., Fatemi, E.: Nonlinear total variation based noise removal algorithms. Physics D **60**, 259–268 (1992)
7. Vogel, C.R., Oman, M.E.: Iterative methods for total variation denoising. SIAM J. Sci. Comput. **17**, 227–238 (1996)
8. Zhu, J.G., Hao, B.B.: A new noninterior continuation method for solving a system of equalities and inequalities. J. Appl. Math. **2014**, Article ID 592540 (2014)
9. Yu, J., Li, M., Wang, Y., He, G.: A decomposition method for large-scale box constrained optimization. Appl. Math. Comput. **231**(12), 9–15 (2014)
10. Han, C., Feng, T., He, G., Guo, T.: Parallel variable distribution algorithm for constrained optimization with nonmonotone technique. J. Appl. Math. **2013**, Article ID 295147 (2013)
11. Sun, L., He, G., Wang, Y.: An accurate active set newton algorithm for large scale bound constrained optimization. Appl. Math. **56**(3), 297–314 (2011)
12. Zheng, F., Han, C., Wang, Y.: Parallel SSLE algorithm for large scale constrained optimization. Appl. Math. Comput. **217**(12), 5277–5384 (2011)
13. Zhu, J., Hao, B.: A new smoothing method for solving nonlinear complementarity problems. Open Math. **17**(1), 21–38 (2019)
14. Tian, Z., Tian, M., Gu, C.: An accelerated jacobi gradient based iterative algorithm for solving sylvester matrix equations. Filomat **31**(8), 2381–2390 (2017)
15. Chambolle, A.: An algorithm for total variation minimization and applications. J. Math. Imaging Vis. **20**(1–2), 89–97 (2004)
16. Wang, Y., Yang, J., Yin, W., et al.: A new alternating minimization algorithm for total variation image reconstruction. SIAM J. Imaging Sci. **1**(3), 248–272 (2008)
17. Zhang, R.Y., Xu, F.F., Huang, J.C.: Reconstructing local volatility using total variation. Acta Math. Sin. Engl. Ser. **33**(2), 263–277 (2017)
18. Bai, Z.B., Dong, X.Y., Yin, C.: Existence results for impulsive nonlinear fractional differential equation with mixed boundary conditions. Bound. Value Probl. **2016**, 63 (2016)
19. Wang, Z.: A numerical method for delayed fractional-order differential equations. J. Appl. Math. **2013**, 256071 (2013)
20. Wang, Z., Huang, X., Zhou, J.P.: A numerical method for delayed fractional-order differential equations: based on G-L definition. Appl. Math. Inf. Sci. **7**(2), 525–529 (2013)
21. Zhang, Y.L., Lv, K.B., et al..: Modeling gene networks in Saccharomyces cerevisiae based on gene expression profiles. Comput. Math. Methods Med. **2015**, Article ID 621264 (2015)
22. Lu, X., Wang, H.X., Wang, X.: On Kalman smoothing for wireless sensor networks systems with multiplicative noises. J. Appl. Math. **2012**, 203–222 (2012)
23. Ding, S.F., Huang, H.J., Xu, X.Z., et al.: Polynomial smooth twin support vector machines. Appl. Math. Inf. Sci. **8**(4), 2063–2071 (2014)
24. Goldfarb, D., Yin, W.: Second-order cone programming methods for total variation based image restoration. SIAM J. Sci. Comput. **27**(2), 622–645 (2005)
25. Han, C.Y., Zheng, F.Y., Guo, T.D., He, G.P.: Parallel algorithms for large-scale linearly constrained minimization problem. Acta Math. Appl. Sin. Engl. Ser. **30**(3), 707–720 (2014)
26. Hao, B.B., Zhu, J.G.: Fast L1 regularized iterative forward backward splitting with adaptive parameter selection for image restoration. J. Vis. Commun. Image Represent. **44**, 139–147 (2017)
27. Morini, B., Porcelli, M., Chan, R.H.: A reduced Newton method for constrained linear least squares problems. J. Comput. Appl. Math. **233**, 2200–2212 (2010)
28. Chan, R.H., Tao, M., Yuan, X.: Constrained total variation deblurring models and fast algorithms based on alternating direction method of multipliers. SIAM J. Imaging Sci. **6**(1), 680–697 (2013)
29. Huang, Y.M., Ng, M.K., Wen, Y.W.: A fast total variation minimization method for image restoration. Multiscale Model. Simul. **7**(2), 774–795 (2008)
30. Liu, J., Huang, T.Z., et al..: An efficient variational method for image restoration. Abstr. Appl. Anal. **2013**, 213536 (2013)
31. Chambolle, A., Lions, P.L.: Image recovery via total variation minimization and related problems. Numer. Math. **76**, 167–188 (1997)
32. Chan, T., Marquina, A., Mulet, P.: High-order total variation-based image restoration. SIAM J. Sci. Comput. **22**(2), 503–516 (2000)
33. Lv, X., Song, Y., Wang, S., et al.: Image restoration with a high-order total variation minimization method. Appl. Math. Model. **37**, 8210–8224 (2013)

34. Liu, G., Huang, T., Liu, J.: High-order TVL1-based images restoration and spatially adapted regularization parameter selection. Comput. Math. Appl. **67**, 2015–2026 (2014)
35. Zhu, G.J., Li, K., Hao, B.B.: Image restoration by a mixed high-order total variation and l1 regularization model. Math. Probl. Eng. **2018**, Article ID 6538610 (2018)
36. Lysaker, M., Tai, X.C.: Iterative image restoration combining total variation minimization and a second-order functional. Int. J. Comput. Vis. **66**(1), 5–18 (2006)
37. Zhu, J., Liu, K., Hao, B.: Restoration of remote sensing images based on nonconvex constrained high-order total variation regularization. J. Appl. Remote Sens. **13**(2), 022006 (2019)
38. You, Y.L., Kaveh, M.: Fourth-order partial differential equations for noise removal. IEEE Trans. Image Process. **9**(10), 1723–1730 (2000)
39. Hajiaboli, M.R.: An anisotropic fourth-order diffusion filter for image noise removal. Int. J. Comput. Vis. **92**(2), 177–191 (2011)
40. Chen, D., Chen, Y., Xue, D.: Fractional-order total variation image denoising based on proximity algorithm. Appl. Math. Comput. **257**, 537–545 (2015)
41. Wang, Z., Xie, Y., Lu, J.,et al..: Stability and bifurcation of a delayed generalized fractional-order prey–predator model with interspecific competition. Appl. Math. Compt. **347**, 360–369 (2019)
42. Wang, X., Wang, Z., Huang, X.,et al..: Dynamic analysis of a fractional-order delayed SIR model with saturated incidence and treatment functions. Int. J. Bifurcat. Chaos **28**(14), 1850180 (2018)
43. Jiang, C., Zhang, F., Li, T.: Synchronization and antisynchronization of N-coupled fractional-order complex systems with ring connection. Math. Methods Appl. Sci. **41**(3), 2625–2638 (2018)
44. Ren, Z., He, C., Zhang, Q.: Fractional order total variation regularization for image super-resolution. Signal Process. **93**(9), 2408–2421 (2013)
45. Wu, C., Tai, X.C.: Augmented Lagrangian method, dual methods, and split Bregman iteration for ROF, vectorial TV, and high order models. SIAM J. Imaging Sci. **3**(3), 300–339 (2010)
46. Michael, N., Chan, R.H., Tang, W.C.: A fast algorithm for deblurring models with Neumann boundary conditions. SIAM J. Sci. Comput. **21**(3), 851–866 (1999)
47. Gonzalez, R.C., Woods, R.E.: Digital Image Processing, 3rd edn. Prentice Hall, New York (2011)
48. Yang, J.F., et al.: A fast algorithm for edge-preserving variational multichannel image restoration. SIAM J. Imaging Sci. **2**, 569–592 (2011)
49. Wang, Z., Bovik, A.C., Sheikh, H.R., Simoncelli, E.P.: Image quality assessment: from error visibility to structural similarity. IEEE Trans. Image Process. **13**, 600–612 (2004)